공학석사학위논문

Implantable Buckled Cell-Graphene Device for Diagnosis of Muscular Disorder

근육질환진단을 위한 이식형 세포-그래핀 디바이스

2016년 01월

서울대학교 대학원

화학생물공학부

조경원

Abstract

Implantable Buckled Cell-Graphene Device for Diagnosis of Muscular Disorder

Kyoung Won Cho

School of Chemical and Biological Engineering

The Graduate School

Seoul National University

Implantable medical device to diagnose muscular disorder by recording electrophysiological signals of muscle tissue has been actively used in clinical medicine. However, mechanical mismatch between conventional rigid wafer-based medical device and soft curvilinear muscle tissue brings a low signal and muscle damage during implantation. Soft and flexible biocompatible medical device for recording signals of muscle tissue while preventing muscle damage during implantation is critical issue in implantable medical device. Here, we developed a soft implantable buckled cell-graphene medical device that can be safely implanted on top of muscle tissue and record electromyographic signals

for diagnosis. The buckled cell-graphene is comprised of mesh-patterned graphene electrodes on buckled topology of polydimethylsiloxane with C2C12 myoblast sheet placed on top of the electrodes. The buckled topology was constructed *via* controlling the thickness of polyimide membrane which is placed on below of the electrodes. The buckled topology results cell alignment of C2C12 myoblast mimicking a nature orientation of muscle tissue. Mesh-patterned graphene electrodes serve as a cell culture substrate enhancing proliferation and differentiation of the cells, while serving as eletromyography sensor to record electrophysiological signals of muscle tissue *in vivo*. Additionally, C2C12 myoblast of cell-graphene device provides cellular therapeutic effect during *in vivo* implantation without immune response.

Keywords: buckled graphene, stretchable electronics, implantable device, electrophysiology, electromyography

Student number: 2014-21598

Contents

List of Schemes

List of Figures

1. Introduction

Measurement of electrophysiological signals from muscle tissue is important in diagnosis of muscular disease derived from muscle and/or motor neuron dysfunctions.[1] Continuous monitoring of electromyography (EMGs) for a variety of neuromuscular disorders, especially muscular lesion including abnormal muscular contraction[2], spasticity[3], and sarcopenia[4], and the immediate actions such as electrical stimulation[5,6] for controlling those symptoms are needed. Medical devices related to muscle disorder in which measure on skin has been developed[7], yet implantable one has advantages in high resolution and precise measurement of electrophysiological signals coming from target muscle tissue.[8] The medical devices related to neuromuscular disorders in the past were fabricated as types of wire, and microchip, and metal-pad.[9] These devices, however, were fabricated with rigid metal electrodes[10] which had limitations in conformal contact of sensor with curved surface of muscle tissue[11,12] and obstruction in muscular movements such as stretching and compressing. Furthermore, the rigidity of conventional implantable devices may cause damage in muscular tissue during muscular movement which may leads to scarring[13], and brings

inconvenience to patients. To overcome these limitations, flexible and stretchable implantable medical devices[14-16] are necessary and have been developed not only for muscle but also for other organs such as brain[17] and cardiac[18].

Meanwhile, long term implantation of medical devices had been remained as limited due to poor biocompatibility and cytotoxicity, and lack of therapeutic functionality. Loading drugs on implantable medical device has been interest for its therapeutic effect.[19,20] Incorporation of drug within implantable medical device, however, is difficult to be fabricated in terms of complexity and requires reloading of drug for its short duration of drug effect.[21,22] Implantation of medical devices coated with the culturing cells equivalent to target organ reduces immune response and prevents reduction of sensor resolution[23], as well as provides therapeutic effect of cells. Cell therapy, a promising tool in tissue engineering and regenerative medicine for treatment of damaged tissues, is actively studied[24,25] and used in treatment of a variety of organs such as brain[26], heart[27], and muscle[28].

Here, we introduce a stretchable and transparent buckled cell-graphene hybrid comprised of C2C12 myoblast for a target organ of implantation, mesh-patterned graphene nanomembrane, and sub-micron

polyimide (PI) membrane on a biocompatible polydimethylsiloxane (PDMS) elastomer (Scheme 1). Mesh patterned graphene nanomembrane promotes proliferation and differentiation of muscle cells and serves as electrodes of electromyography sensor for monitoring electrophysiological behavior of muscle tissue and *in vivo* electrical stimulator. The size of wavy surface of buckled device on elastomer substrate is dependent on thickness of PI membrane.[29] The wavy structure enhances stretchability[30] of the device in which is critical for preventing its deformation during the state of implantation from muscular movements. This cell-graphene hybrid has four major functions: (i) culturing cells aligned with anisotropic pattern of buckled surface for mimicking native muscle tissue, (ii) monitoring electrophysiological behavior of muscle tissue *in vivo* continuously *via* mesh patterned graphene, (iii) serving as *in vivo* implantable medical device for electrical stimulator, and (iv) providing cell sheet therapy on hindlimb muscle tissue.

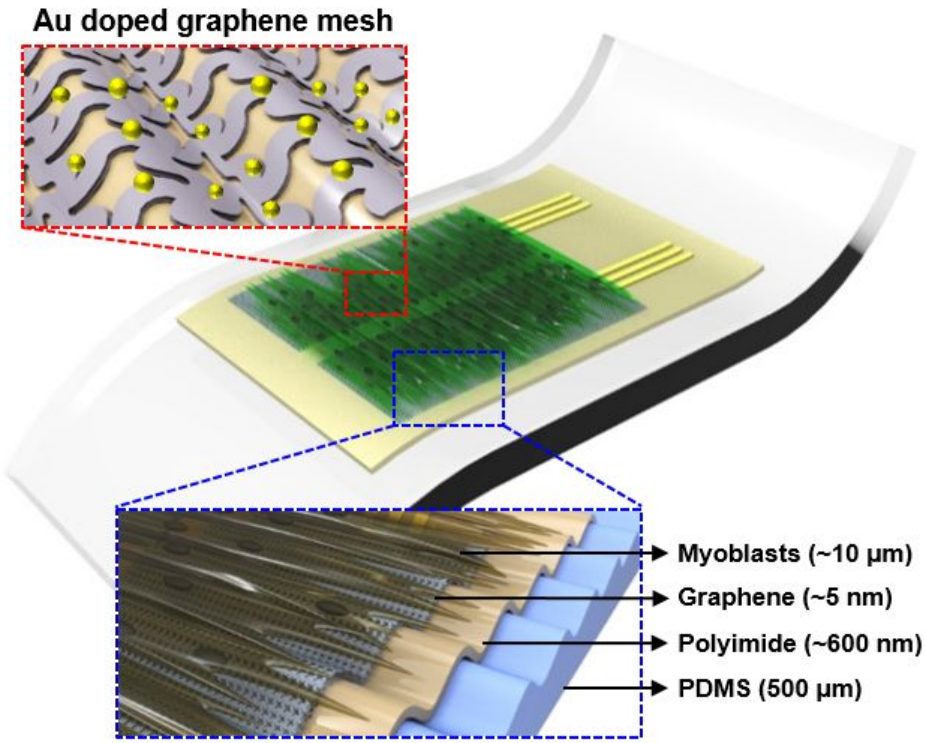

Scheme 1 Overview of the architecture of the stretchable and transparent buckled cell-graphene hybrid

2. Stretchable and buckled implantable device with serpentine mesh-patterned graphene electrodes and cell sheet

2.1 Fabrication of implantable buckled cell-graphene device

Our system mainly consists of serpentine mesh-patterned graphene electrodes to serve as enhanced cell substrates for C2C12 myoblast as well as electrodes for electromyography sensor. This graphene electrodes are placed on buckled topology of PI/PDMS substrate, enabling to be stretched as muscle tissue move during implantation. Also, along with the wavy structure of buckling topology, C2C12 myoblasts are cultured on top and express uniaxial alignments as muscle fibers do. This cell sheet of C2C12 myoblast brings high quality of biotic/abiotic interface during EMG measurement with graphene electrodes. As

seen in Scheme 2, Au membrane for connecting electrodes is patterned on Ni layer-deposited silicon wafer. Then, copper graphene sheet grown by chemical vapor deposition process is placed on and patterned into serpentine mesh with photolithography process. On another Ni layer-deposited silicon wafer, PI membrane is coated. Serpentine mesh-patterned graphene electrodes and Au connective electrodes are transferred onto top of the PI membrane. Next, Ni layer under the PI layer is etched away, so all three layers including graphene electrodes, Au connective electrodes and PI layers can be transferred onto a stretched PDMS. Then, the stretched PDMS is released so the graphene electrodes and the PI layer form buckling structure. After sterilization of the device, C2C12 myoblasts are cultured on top of the device to achieve fabrication of implantable buckled cell-graphene device. Each components of this device was designed and plays important role for its device to be utilized as implantable medical device.

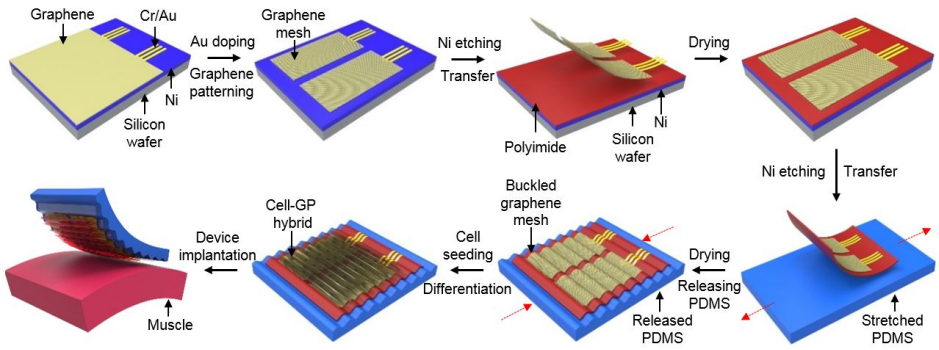

Scheme 2 Fabrication process and key applications *in vivo* of the implantable buckled cell-graphene device

2.2 Controlling buckled topology

While a high resolution sensor for medical device is a critical factor, mechanical properties of a medical device, especially for implantation, is another important factor. The material of a medical device can be soft or stretchable. Tissue like skeletal muscle in our body stretches itself. Nevertheless, some parts of our organs such as GI tract or esophagus, where it needs to be stretched more than its original mechanical properties contain buckling structure. To devise such an extra stretchable and soft implantable device to minimize discomfort during implantation, we employed buckling feature in our implantable cell graphene device. The buckling topology of the device is achieved by controlling the thickness of PI membrane placed on top of a PDMS**.** PI membranes with different thickness are placed on a stretched PDMS and the PDMS is released. With respect to the thickness of PI membrane, the size of buckling topology results differently. (Figure 1) The thickness of PI membrane

is controlled by diluting PI with its solvent N-Methyl-2-Pyrrolidone (NMP) concentration. As seen in Figure 2a, the thickness of PI membrane is decreased as the concentration of PI decrease. The thickest membrane is 1.4μm in 12 wt% polyimide/NMP. The thinnest membrane is 0.3μm in 2 wt% concentration. This difference in thickness causes on the total buckling sizes when each membranes is placed on top of the stretched PDMS. PDMS is stretched 30% which is more than native muscle tissue can be stretched[31,32]. As seen in Figure 2b, the wavelength of buckling topology is decreased as PI/graphene thickness decreases. The largest wavelength is 183μm in 1.4μm thickness of PI/graphene, and the lowest one is 8μm in 0.3μm thickness of PI/graphene membrane. The buckling topology of PDMS, which is the main platform of the device can be simply controlled by changing the thickness of PI membrane. While metal electrodes placed on top of a flat PDMS cannot maintain their electrical properties during stretching state, those placed on buckled structure can maintain.

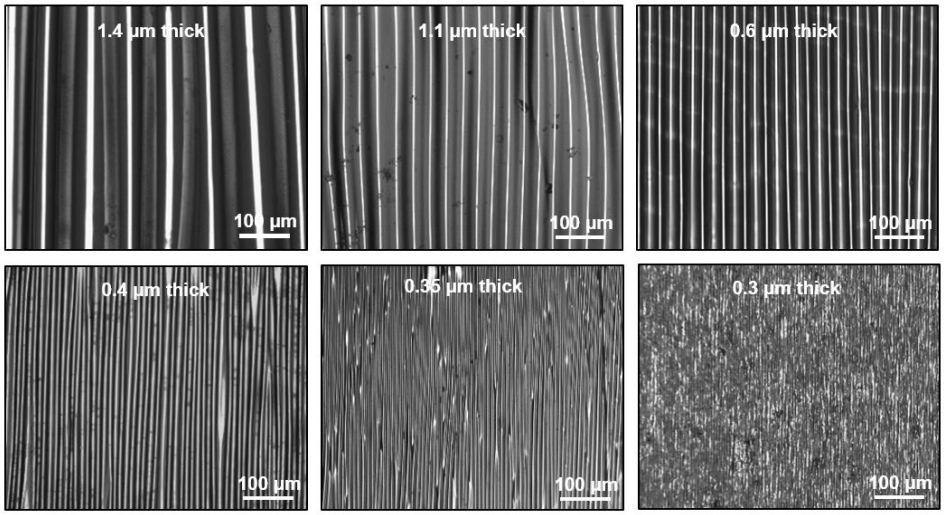

Figure 1 Optical microscopic images of uniform buckled structure of different wavelengths according to the PI/graphene layer thickness (from 1.4 μm to 0.3 μm)

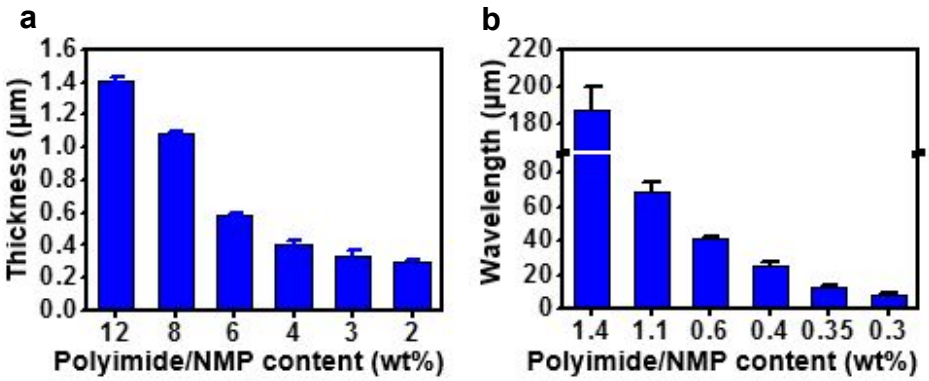

Figure 2 Characterization of buckling topology in respect to polyimide/NMP contents for (a) thickness and (b) wavelength

2.3 Optimization of buckled topology for cellular alignments

Naturally, muscle fibers in our body are uniaxial aligned. Mimicking its direction property of muscle fiber, *in vitro* muscle cells can be also aligned when it is cultured on buckling topology. Buckling provides stretchability of the device as well as cellular alignments. To evaluate the cellular alignment, C2C12 myoblast is cultured on the buckled device with different wavelengths, and is observed using fluorescence microscopy. As seen in Figure 3, actin filaments and nuclei directions in each different buckled topology can be observed. All samples contains uniaxial direction, compared to control sample, which is cultured on a conventional cell culture plate. The directions of nuclei are analyzed and their alignment ratios are plotted in Figure 4. The highest alignment ratio (98%) is obtained when C2C12 myoblast is cultured on the buckling topology of 41μm wavelength, whereas both C2C12 myoblasts

cultured on 187μm wavelengths and culture plate as control show the lowest alignment ratios, 19% and 17%, respectively. Different wavelength of buckling topology provides different cellular alignment ratio. The wavelength of 187μm buckling is too large for the cells to recognize the buckling topology. All buckling sizes except the wavelength of 187μm show at least 70% alignment ratio. Nevertheless, the wavelength of 41μm is selected to implement in our device to mimic native muscle fiber as much as possible. Differentiation of myotube formation is validated. (Figure 5)

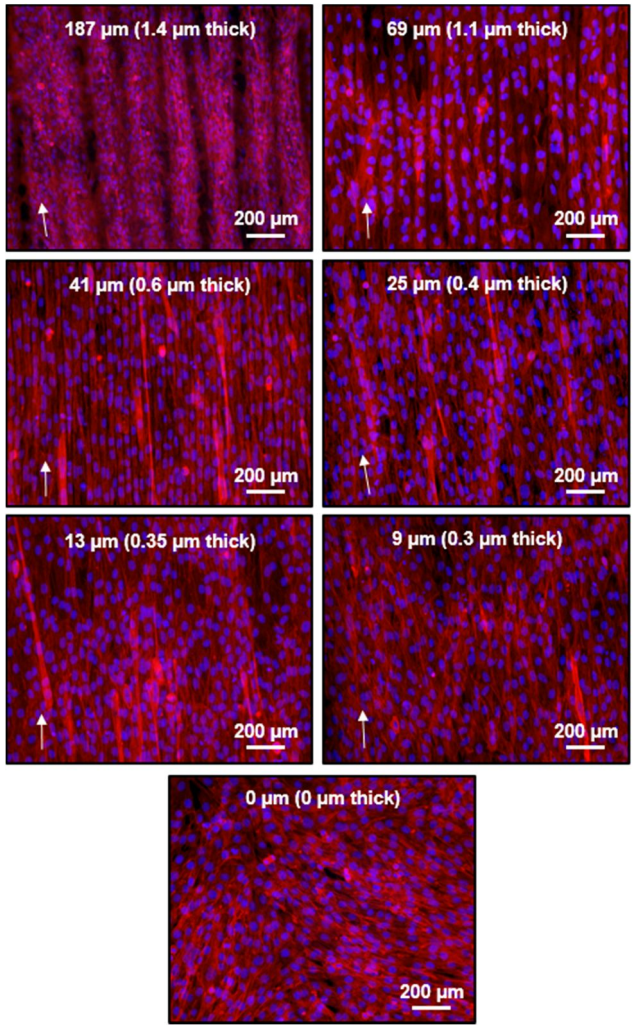

Figure 3 Fluoresce microscopic images of cell alignments in respect to the wavelengths of anisotropic buckled graphene mesh

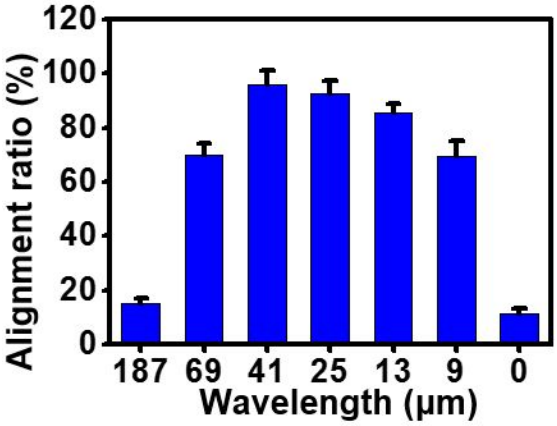

Figure 4 A plot of cell alignment ratio percent versus buckling wavelengths

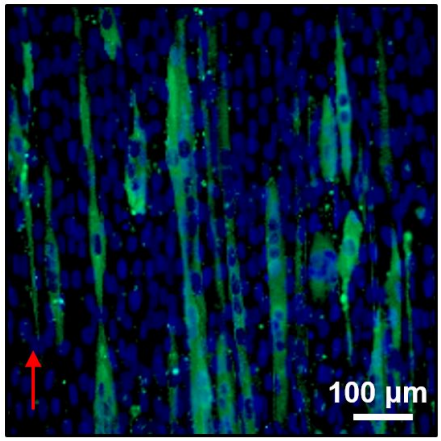

Figure 5 Fluorescence image of myotube formation with alignments

3. Mechanical aspects of implantable buckled cell-

graphene device

3.1 Soft and stretchable medical device mimicking muscle tissue

Muscle tissue contains movements of stretching and compressing. With combination of stretching and compressing, muscle tissue also can be twisted. Particularly, muscle tissue experience much larger movements than other tissue such as brain or bone. Skeletal muscle, especially, can be controlled by a person's conscious. It is inevitable not to use skeletal muscle for hours when long term EMG sensing is needed. Conventional rigid implantable device brings discomfort to patients. Moreover, it can bring damage on muscle tissue and low signals of EMG sensing during implantation because of muscular movements. Implantable device that is soft and stretchable to minimize discomfort while maintaining its EMG sensing performance and its abiotic/biotic interface is needed. Our device, as seen in Figure 6a, is soft and flexible that can be stretched and twisted, so the muscle movements are not an issue during implantation. Also, the graphene electrode is designed as serpentine mesh to provide stretchability. All materials used in this device are biocompatible and lessens discomfort to patients during implantation compared to conventional rigid implantable medical devices.

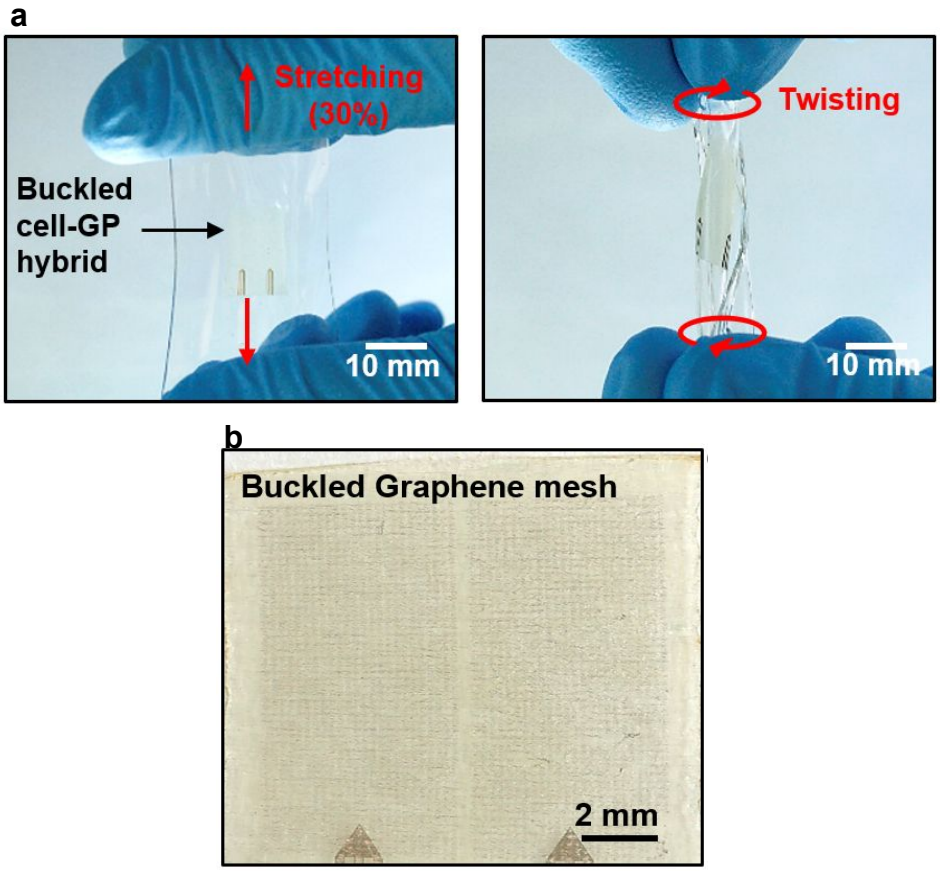

Figure 6 Images of the implantable buckled cell-graphene device during (a) uniaxial stretching and twisting, and of (b) mesh-patterned graphene electrodes

3.2 Stretching, compressing, and bending tests

Even if the device is very stretchable or flexible, the electrode of device must maintain its property such as conductance or resistance under stretching or compressing state. Otherwise, the device cannot properly function under stretching or compressing conditions of muscular movements. We devised stretchable implantable device for reading electrophysiological signals of muscle tissue. To evaluate if the EMG sensor work properly under stretching, compressing or bending condition, the resistance of buckled mesh patterned graphene (buckled mesh) electrode is measured during the above three conditions. For comparison of our buckled cell-graphene device, non-patterned graphene sheet without buckling sample (flat sheet) and buckled but non-patterned graphene sheet (buckled sheet) are also tested as control experiment. The resistance of each samples is measured under stretching state. In Figure 7, the resistance of flat sheet sample is dramatically increased right after stretching begins and only lasts for 5% stretching. Graphene intrinsically can be stretched[34], so this result complies with the reference. On the other hand, the resistance of buckled sheet sample is relatively stable until stretching of 22% and begins to rise. At stretching state of 30%, the electrode of buckled sheet is broken. The resistance of buckled sheet can be stable because of the structural design, buckling. As stretching occurs, the buckled topology flattens and the resistance change is not affected. The strain distribution of on buckled sheet is studied as shown in Figure 8a. According to the strain distribution, the peak of

wavelength in buckling topology contains the most strain percent and the strain is released as the buckling topology flattens by stretching. The resistance of our buckled mesh sample is steady for up to stretching of 35%, which is much better than that of buckled sheet, and lasted more than 40% stretching until it is broken. Compared to the buckled sheet, the pattern of graphene provides additional support of stretching. Mesh pattern of graphene provides additional 10% stretching while maintaining the performance of electrode. In Figure 8b, the strain distribution shows that the maximum strain on mesh-patterned graphene electrodes, especially on the peak was 10.7% at 0% stretching and became 0% at 30% stretching, but gained back after 40% stretching. Likewise, the results of strain distribution study on stretching tests of buckled sheet and buckled mesh are consistent with the experimental results. The combination of buckling topology and graphene mesh pattern support our device to be utilized as implantable medical device on muscle. The maximum stretching of muscle tissue is 30%[33] in which is much less than our stretching test condition. Our device, under any muscular stretching conditions, is stable and can read electrophysiological signals of muscle tissue during implantation. In compressing test, the resistances of all three samples are measured as the above stretching test. (Figure 9a) Unlike stretching test of flat sheet sample, the resistance of flat sheet gradually increases as compressing occurs, and lasts until 18% compressing. The electrodes of buckled sheet and buckled mesh are broken at 31% and 36% compressing ratios, respectively. In compressing test, the

maximal compressing ratio for buckled mesh is more than that of buckled sheet, yet the difference between two samples at compressing test is only 5% which is less the difference at stretching test which is more than 10%. Nevertheless, the buckled mesh is more suitable and stable for implantation since muscle tissue can be compressed not more than 15%.[33] Since muscle can also be twisted, we performed bending test on all three samples. (Figure 9b) Each sample is bended for up to 90 degrees and its resistance is measured at each angle. Interestingly, the electrode of buckled mesh is stable throughout the test. However, the electrodes of flat sheet and buckled sheet are broken at 20 degrees and 60 degrees, respectively. The resistance of flat sheet is increased as soon as it is bended, but that of buckled sheet is stable for up to 40 degrees bending. All three tests including stretching, compressing, and bending tests support the goal of our buckled mesh patterned device as implantable while stable medical device to diagnose muscular disorders.

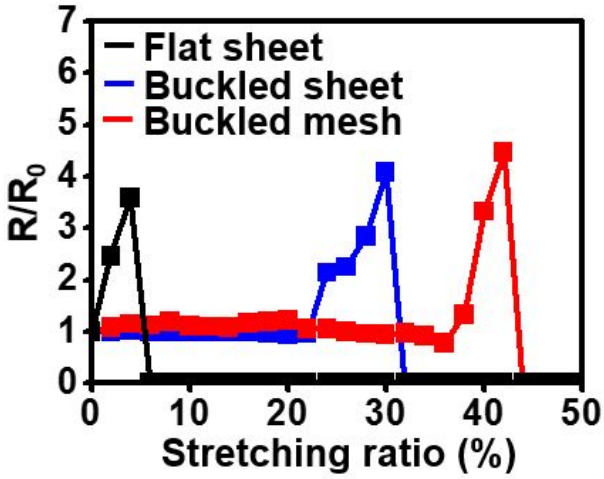

Figure 7 Maximal endurance tests of three samples including flat sheet, buckled sheet, and buckled mesh during stretching condition

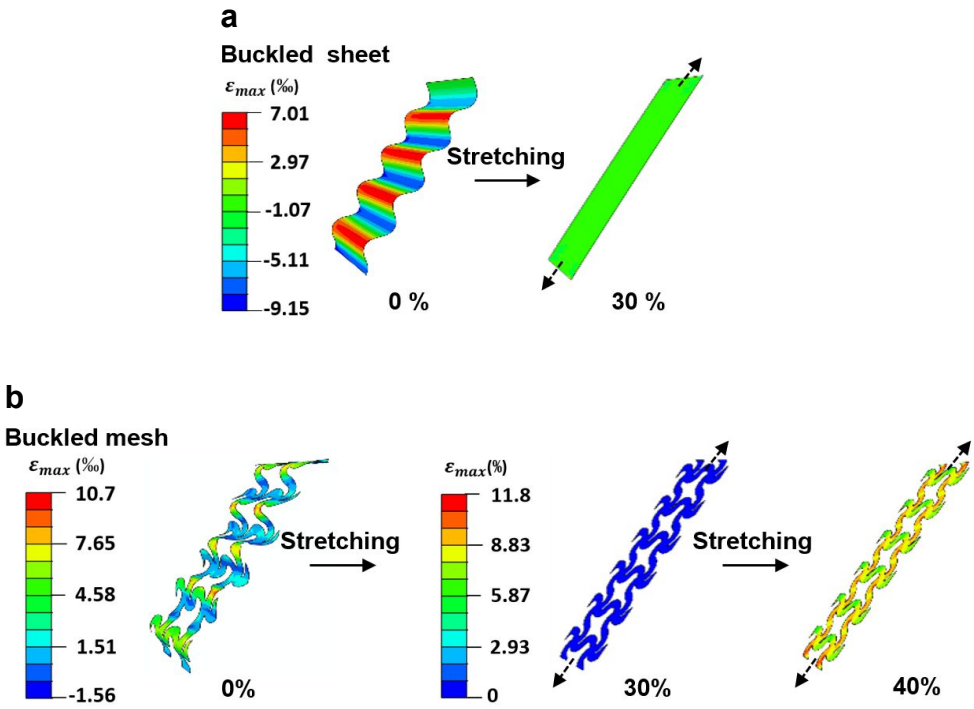

Figure 8 Strain distributions of (a) a buckled sheet and (b) a buckled mesh during stretching conditions

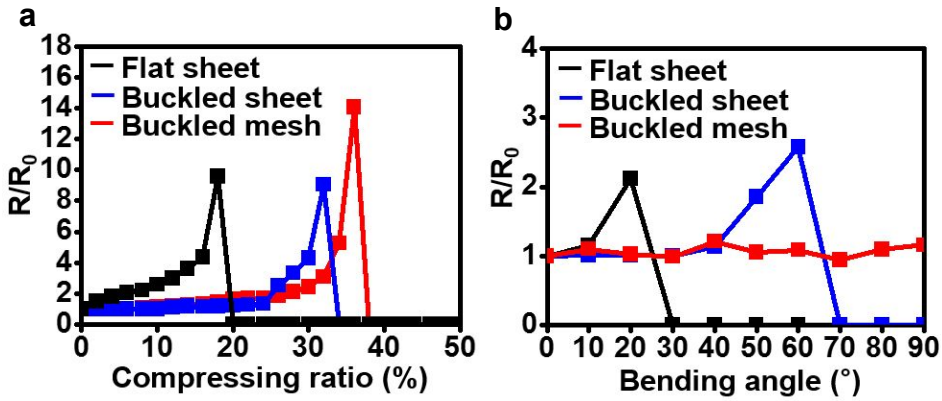

Figure 9 Maximal endurance tests during (a) compressing and (b) bending conditions

3.3 Electrical hysteresis of the device

The mechanical reliability of graphene electrode during stretching or compressing condition is an important factor in implantable medical device. Even if the device can stretch or compress, the electrode that cannot mechanically withstand multiple stretching or compressing conditions is useless to be utilized as a medical device. To evaluate the mechanical reliability of the device, we recorded the resistance of graphene electrode during stretching and compressing condition by applying bending stress at 30^{o}. (Figure 10a) The line of least resistance of graphene mesh electrode from top to bottom is measured. The bending stresses of stretching and compressing are performed 10,000 cycles each. As seen in Figure 10b, the line of least resistance for the graphene mesh was maintained at approximately 8,000 Ω for over 10,000 cycles of both stretching and compressing conditions. This experiment shows that our buckled cell-graphene device is electrically reliable and mechanically stable under the conditions of multiple stretching or compressing.

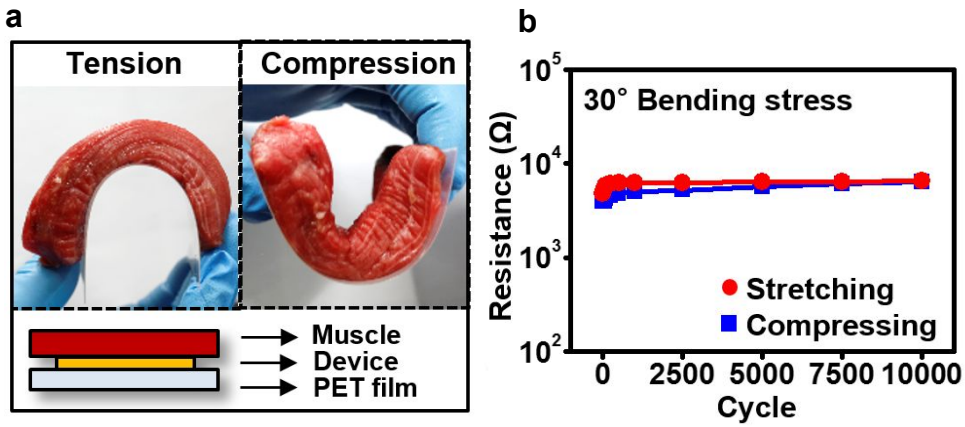

Figure 10 Fatigue cycling test of the implantable buckled cell-graphene device

(a) testing process, (b) test result

4. Au-doped serpentine mesh-patterned graphene

electrode and its electrochemical characterization

Our buckled graphene mesh electrodes have been doped with Au particles in order to enhance electrochemical characterization. Simple process of Au doping was implemented on the buckled graphene mesh by spin coating method as seen in Scheme 3. Au doping process greatly enhances the electrochemical properties of our device as compared to non-doped buckled graphene mesh. The impedance and conductance of 4 different sample electrodes including flat graphene mesh, buckled graphene mesh, Au-doped and buckled graphene mesh, and flat Au mesh are measured under PBS solution. In Figure 11a, the impedance is significantly increased from graphene mesh to buckled graphene mesh. Structural modification, buckling, itself affects negatively on electrochemical property of graphene mesh. However, Au doping process greatly lowers its impedance value very close to that of flat Au mesh. Au doping also enhances the conductance of buckled graphene mesh electrodes. As seen in Figure 11b, the conductance of buckled graphene mesh shows the lowest, yet Au-doped buckled graphene mesh shows higher conductance than that of flat graphene mesh. To evaluate whether material maintain its original electrochemical properties under bio-fluidic environment, impedances of those

4 different samples are measured under growth medium for 7 days. (Figure 12) All samples well maintain their electrochemical properties for 7 days. In other words, the electrochemical property of our Au-doped buckled graphene mesh electrodes do not alter during implanted environments.

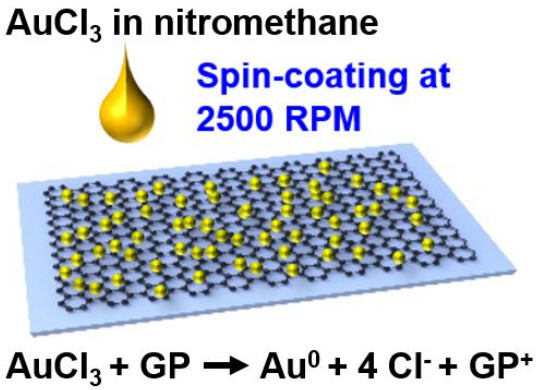

Scheme 3 Au doping process

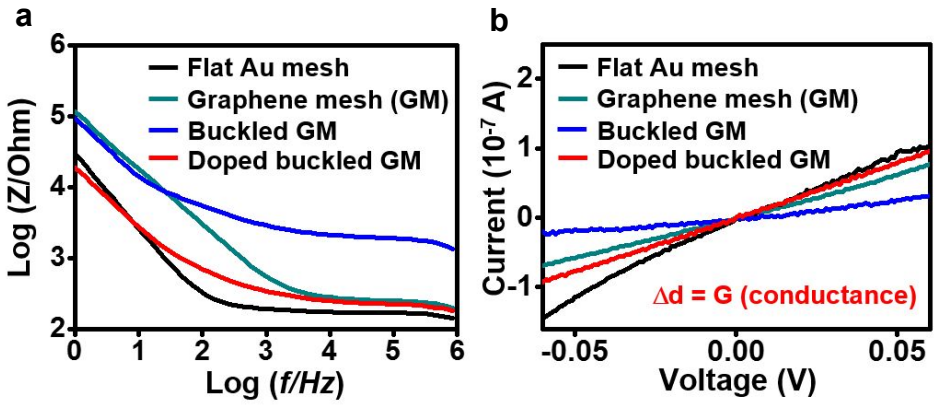

Figure 11 Electrochemical characterizations of (a) impedance and (b) conductance

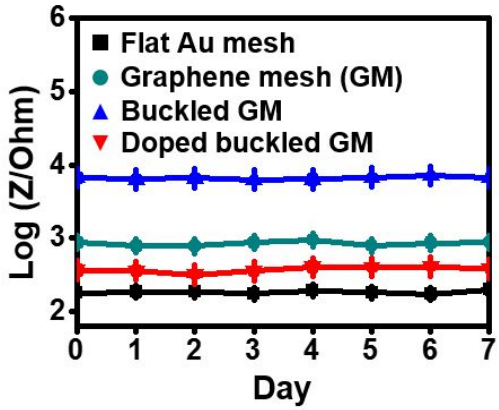

Figure 12 A plot of impedance change for 7 days in PBS solution

5. Electromyography Sensor

5.1 Testing EMG sensor *ex vivo*

Applicability of the buckled graphene mesh electrodes as electromyography sensor is evaluated by testing recording and stimulating efficiencies on *ex vivo* model. Figure 13a shows a photographic image of buckled graphene mesh implanted on bovine muscle *ex vivo*. The stimulating and recording efficiencies are evaluated as described in a schematic illustration of Figure 13b. Buckled cell-graphene device is placed on top of bovine muscle and Au electrode is placed on bottom of the muscle. For recording efficiency, 1 V electrical signal is applied from Au electrode and its signal is read by the device at each depth of the muscle. As seen in Figure 14a, the recording efficiency is decreased as the measured depth of muscle is increased, but its efficiency curve becomes plateau after 15 mm of muscle depth. The recording efficiency does not decrease below 86% even measured at 30 mm of muscle depth. Electrical stimulation is another important mode of implantable device for therapeutic application of muscular disorder. Its stimulating efficiency is also evaluated on *ex vivo* model. (Figure 14b) 1 V signal is generated by the buckled cell-graphene device and its signal

is measured at each muscle depth by Au electrode. The stimulating efficiency does not decrease below 88% throughout the muscle depths of 30 mm. Evaluation of buckled cell-graphene device on *ex vivo* model show its effectiveness for its usage as implantable electromyography sensor as well as electrical stimulator.

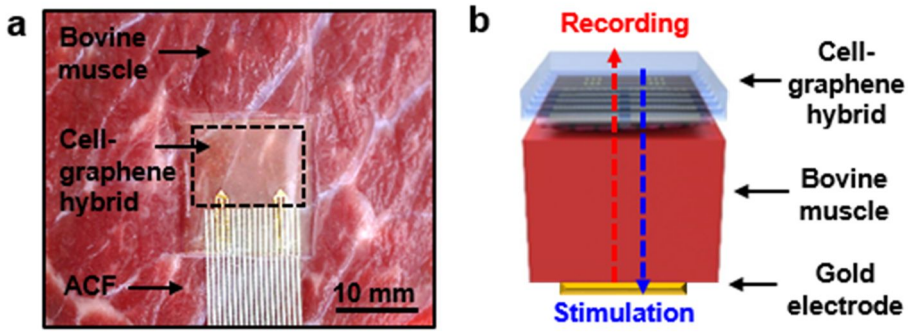

Figure 13 Image of the device implantation onto bovine muscle *ex vivo* (a) and the process of measuring the efficiencies of the device for its recording and electrical stimulation (b)

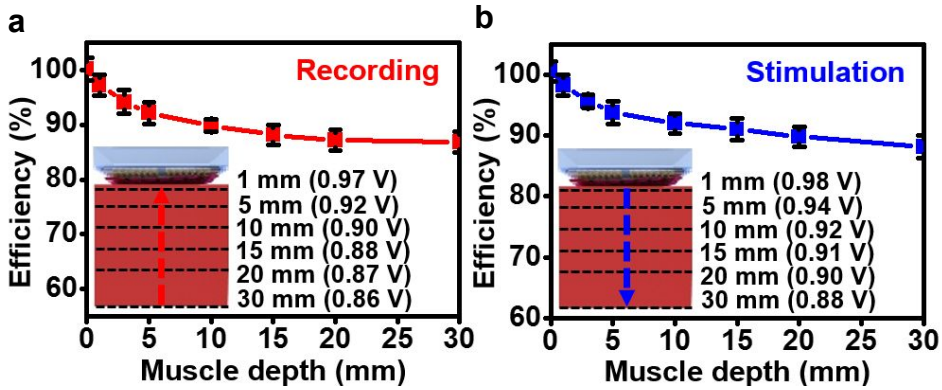

Figure 14 Plots of the efficiencies of the device *ex vivo* for (a) recording and (b) electrical stimulation

5.2 Electrophysiological investigation of EMG sensor *in vivo*

Investigation of electrophysiological applicability of the buckled cell-graphene device *in vivo* is performed by providing electrical signal on and recording electromyography signal of hindlimb muscle of a nude mouse *in vivo*. The device is implanted on hindlimb muscle after excising its skin. (Figure 15) Applying the electrical stimulation, twitching motion of a leg can be observed as shown in Figure 16 top. The number of twitching motion per second corresponds to the value of frequency applied. Electrical stimulation with higher frequency results faster twitching motions. Also, the twisting motion is measured as its electromyography signal is recorded *via* the buckled cell-graphene device. As shown in Figure 16 bottom, two different voltages, 1 V and 0.5 V, with a frequency of 1 Hz are applied and their electromyography signals are measured. The effectiveness of electrical stimulation and electromyography sensing modalities in the buckled cell-graphene device is evaluated. EMG signal of unanesthesized nude mouse is also measured *via* the buckled cell-graphene device. The device is implanted on hindlimb of an anesthesized nude mouse, and the signal of the muscle movement is measured when the mouse is moving after awakening from anesthesia. EMG signal is read at each time a mouse

moves. Its raw EMG signal is shown in Figure 17 top, and its filtered signal is shown in Figure 17 bottom. However, no signal is measured from anesthetized condition. In other words, the EMG signal measured at every movements of unanesthezied mouse is valid against noise signal. *In vivo* investigation shows a promising applications of the buckled cell-graphene device as implantable EMG sensor for diagnosis and as electrical stimulator for therapeutic application.

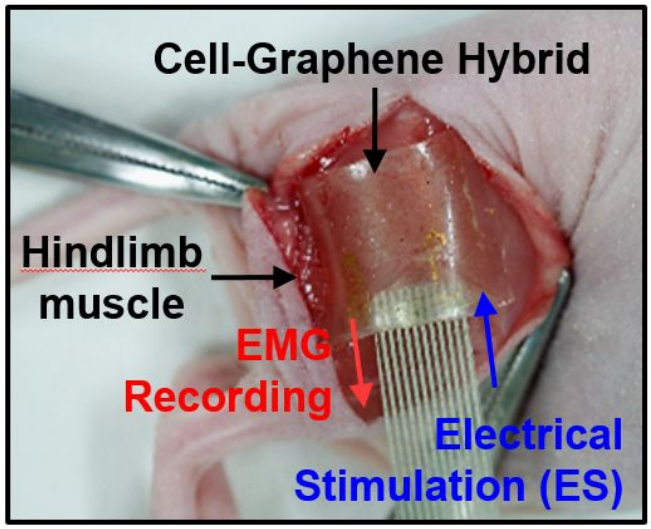

Figure 15 Image of *in vivo* implantation of the device

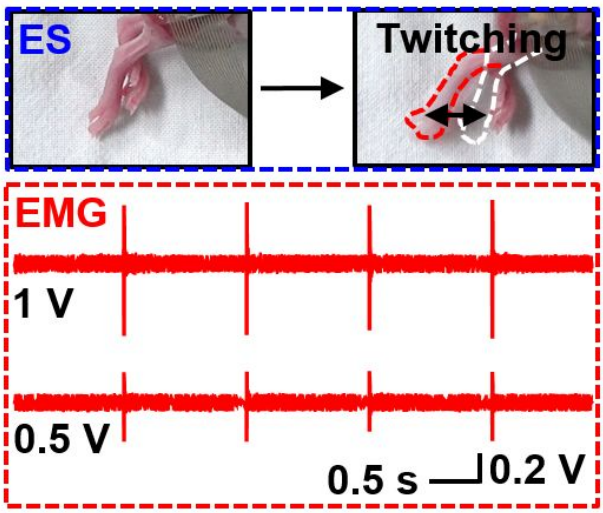

Figure 16 Images of twitches elicited by electrical stimulation from the device (top) and the raw EMG signals from two different electrical signals (bottom)

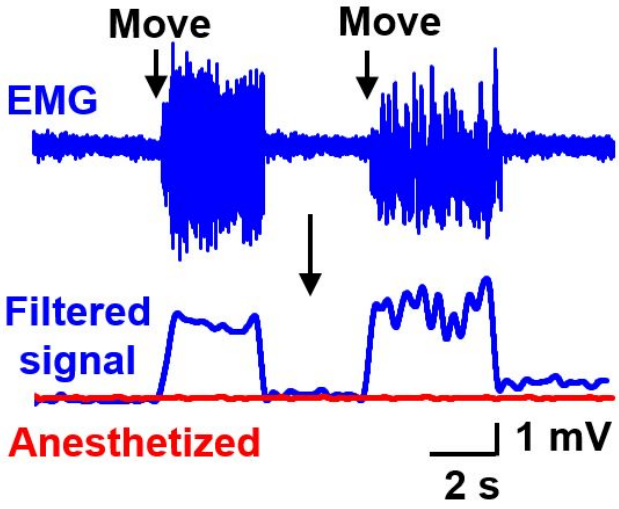

Figure 17 Measurement of the EMG signals by the device on murine hindlimb *in vivo*

6. Therapeutic application of cell sheet

The aligned cell sheet of C2C12 myoblast on buckled cell-graphene device provides therapeutic effect which is applicable in regenerative medicine. The localization of the cells with high density is advantage in a perspective of cell therapy. Muscle fiber-mimicked cell sheet of C2C12 myoblast is transfected with green fluorescent protein (GFP) to observe their activities integrated in the buckled device during implantation. The buckled cell-graphene device with well differentiated GFP-C2C12 myoblast sheet is implanted on a hindlimb muscle of nude mice and was observed *in vivo* using the IVIS Lumina imaging system at 1 day and 7 days after implantation. Figure 18 shows that the cell sheet is capable of maintaining its organization at the operation site. Fluorescence is not detected elsewhere in the body of a nude mouse at 7 days but at operation site. Long term confinement of cells with high density enhance therapeutic effects *in vivo*. Implanted cell sheet integrated with the buckled cell-graphene device proliferates within the implanted site as shown in Figure 19. At 1 day of implantation, a single layer of GFP-C2C12 myoblast can be observed, but multiple layers can be observed in 7 days after the implantation. The promising therapeutic application of cell sheet therapy can be seen with the localized

confinement of cell sheet within the operated site for 7 days and its increase of cell sheet layers.

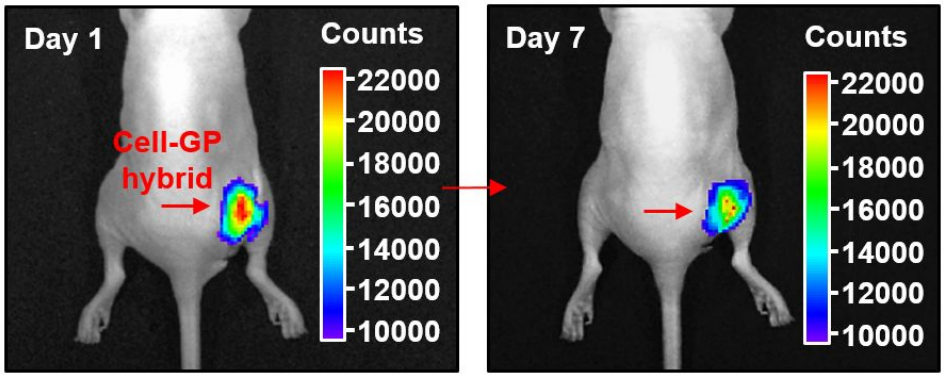

Figure 18 *In vivo* fluorescence images at 1 day and 7 days after the implantation of the device with cell tracers (DiD)

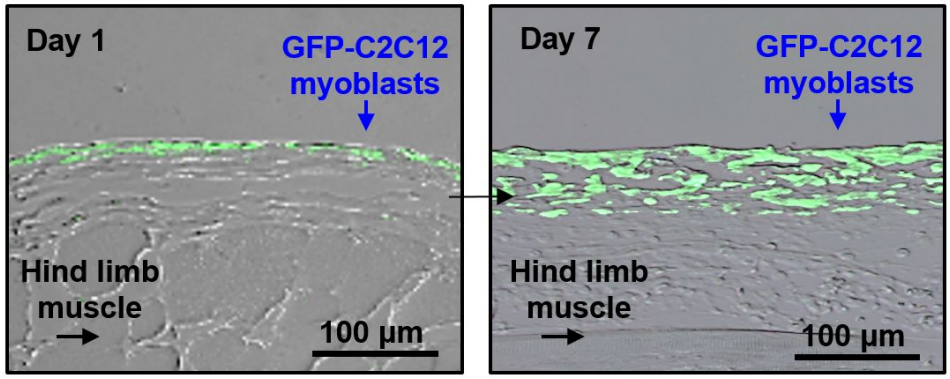

Figure 19 Fluorescence images of GFP-C2C12 myoblasts at 1 day and 7 days after implantation

7. Experimental Section

7.1 Materials

To make buckled cell-graphene device, copper foil (Alfa Aesar), silicon wafer (Si wafer, test grade, 4Science), poly(pyromellitic dianhydride-co-4m4'-oxydianiline)amic acid solution (polyimide, PI, electronic grade, Sigma-Aldrich), polydimethylsiloxane base and curing agent (PDMS, Sylgard 184, Dow Corning), poly(methylmethacrylate) (PMMA, MicroChem), N-Methyl-2-Pyrrolidone (NMP, Sigma-Aldrich), Gold(III) chloride (Sigma-Aldrich), Nitromethane (Samchun chemical), positive photoresist (S1805, MicroChem), acetone (Samchun chemical), methanol (Samchun chemical), isopropyl alcohol (IPA, Samchun chemical) were used

7.2 Detailed fabrication process of buckled topology

40 nm of Ni layer is deposited onto Si test wafer by thermal evaporator. PI

solution is diluted with its solvent NMP into 6 wt% to change the thickness of PI membrane. The diluted PI solution is spin coated on Ni-deposited wafer in 4000 rpm, 60 sec and cured on a hot plate at 150°C and increase the temperature up to 250°C for 90 min. After curing, PMMA is spin coated on the sample. Then, immerse the sample into Ni etchant to etch the Ni layer. After etching Ni layer, PI membrane floats on to Ni etchant solution, and scoop the PI membrane into DI multiple times until Ni etchant is fully washed away. At the final step of washing, use pre-stretched PDMS to scoop the PI membrane and dried in 70°C oven. Next, PMMA layer is removed with acetone, methanol, and IPA. Finally, the stretched PDMS is released. Stretched PDMS is obtained by holding each side of PDMS with binder clips.

7.3 Detailed fabrication process of mesh-patterned graphene electrode

40 nm of Ni layer is deposited on Si test wafer by thermal evaporator. Then, 7nm of chrome for adhesion and 70 nm of Au layer are deposited by thermal evaporator. Au layer is patterned using photolithography process to obtain Au connective electrodes. Copper graphene was grown by chemical vapor deposition process with a mixture of 20 sccm methane gas and 8.4 sccm hydrogen gas under 1000°C. Then, graphene layer is scooped with the above Au

connive electrodes. Graphene is patterned into mesh design by photolithography with photoresist S1805 and etched with reactive ion etching (RIE) using O_2 plasma. After graphene patterning, PMMA is spin coated at 3000 rpm for 30 sec. The sample, then, is immersed in Ni etchant to etch the sacrificial Ni layer at the bottom.

7.4 Characterization of polyimide membrane and buckling size

Varying thickness of PI membrane was measured using atomic force microscopy (AFM). The wavelength of buckling size was measured with microscopic images of buckled topologies obtained by different thicknesses of PI membrane.

7.5 Cell culture

C2C12 myoblasts (CRL-1772; ATCC) was used for aligned cell sheet on buckled graphene mesh device. C2C12 myoblasts was cultured in proliferation medium consists of Dulbecco's modified Eagle's medium (DMEM) supplemented with 10% fetal bovine serum (FBS, Gibco) and 1% penicillin-streptomycin (PS, Gibco) and in differentiation medium consists of DMEM

supplemented with 5% horse serum (Gibco) and 1% PS. The cells were cultured under standard culture conditions of 37°C and 5% CO_2. The cells were seeded at a density of 2 x 10^4 cells/cm^2 for all experiments.

7.6 Observation of cellular aligned characteristic on buckled device

To observe the cellular alignments of cytoskeletal actin filaments, C2C12 myoblasts were counter-stained with rhodamine phalloidine (Life Technologies) and DAPI. The cultured cells were fixed in 4% paraformaldehyde solution (Sigma-Aldrich) diluted in phosphate-buffered solution (PBS) for 10 min and permeabilized in cytoskeleton (CSK) buffer (150mM sucrose, 50mM NaCl, 3 mM $MgCl_2$, 50 mM Trizma-base, and 0.5 % Triton X-100, pH 6.8) for 5 min. Next, the cells were incubated in block buffer for 2 h to block nonspecific binding sites and incubated with paxillin for 1 h at 37°C. The stained samples were observed and captured by a fluorescence microscope (Eclipse Ti, Nikon). On each different wavelengths of buckling, the orientation of nuclei were counted with analyzing the captured image using Image-Pro Plus software (Media Cybernetics).

7.7 Characterization of electrochemical property of Au-doped buckled graphene electrode

Mesh patterned graphene was immersed for 5 min in 20mM $AuCl_3$ in nitromethane solution, spin coated at 2500 rpm for 1 min, and washed with IPA. The impedance and conductance of Au-doped buckled graphene were obtained under pH 7.0 PBS solution with three-electrode configuration (Graphene mesh, Ag/AgCl, and Pt electrode) using electrochemical workstation (CHI660E, CH Instrument).

7.8 *In vivo* mouse model

The experiments on animals for *in vivo* implantation and cell therapy were approved by the Animal Care Committees at Seoul National University Hospital. Six-week-old male BALB/c nude mice were anesthetized by intraperitoneal injection with a mixture of zolazepam and xylazine. The skin was surgically incised to 1.5 cm in the ventral aspect of the right thigh.

7.9 Monitoring electromyography signals *in vivo*

The device was implanted on a hindlimb of a nude mouse to characterize the

buckled cell-graphene device *in vivo*. Monophasic square wave pulses controlled by a function generator was applied on the skeletal muscle for electrical stimulation. The EMG signal of the skeletal muscle was measured using data acquisition (DAQ; National Instruments) connected with the LabView program, in which a voltage amplifier is additionally used. The raw EMG signal was processed using MatLab software.

7.10 *In vivo* model for cellular therapeutic application

To observed cellular confinement of C2C12 myoblast sheet *in vivo*, the buckled device along with cell tracer (DiD)-labeled GFP-expressing cell sheets was implanted on a hindlimb muscle of a nude mouse. Imaging of mice was carried out with an IVIS Spectrum instrument (IVIS, PerkinElmer) in epifluorescence mode equipped with 644 nm and 665 nm filters for excitation and emission, respectively. For immunofluorescence staining, the prepared paraffin sections were dewaxed, hydrated, and treated with 0.01 % protease XXIV (Sigma-Aldrich) in PBS for 20 min at 37°C. The specimens were then stained with primary anti-GFP antibodies (Santa Cruz Biotechnology) according to the manufacturer's instructions. The images were acquired using an inverted fluorescence microscope (DM5500 B, Leica).

8. Conclusion

Stretchable and implantable buckled cell-graphene device provides a new strategy for biocompatible and durable implantable device with multifunctional modalities. Buckling feature offers stretchability as well as alignments of cell sheet integrated within the device. Simple size control of buckling *via* changing PI membrane thickness offers a possibility to implement the feature of alignment with varying types of cells which needs aligned property such as muscle or motor neurons. Softness and biocompatibility are essential features, especially, for implantable medical device to diminish the chance of inflammation at implantation site caused by scarring issue during muscular movement if the device is made of conventional rigid material. For continuous monitoring of electromyography signals of skeletal muscle which require frequent movements, the implantable device that can be stretched, compressed, or twisted is required for high quality sensing system with conformal contact with muscle. Mesh-patterned graphene electrodes doped with Au particle greatly

enhance stretchability of the device with high quality electrochemical property of the electrodes. Also, electrical stimulator and cell sheet provide therapeutic function onto implanted tissues. These advances offer a novel strategy in next generation soft bioelectronics in implantable medical device.

9. Reference

1. Khodagholy, D.; Doublet, T.; Quilichini, P.; Gurfinkel, M.; Lelux, P.; Ghestem, A.; Ismailova, E.; Herve, T.; Sanaur, S.; Bernard, C.; Malliaras, G. G. *Nat. Commun*. **2013**, *4*, 1575.
2. Perry-Rana, S. R.; Housh, T. J.; Johnson, G. O.; Bull, A. J.; Berning, J. M.; Cramer, J. T. *Muscle. Nerve.* **2002**, *26*, 367.
3. Feng, C. J.; Mak, A. F. T. *Electromyogr. Clin. Neurophysiol*. **1988**, *38*, 393.
4. Power, G. A.; Allen, M. D.; Booth, W. J.; Thompson, R. T.; Marsh, G. D.; Rice, C. L. *Age* **2014**, *36*, 1377.
5. Minev, I. R.; Musienko, P.; Hirsch, A.; Barraud, Q.; Wenger, N.; Moraud, E. M.; Gandar, J.; Capogrosso, M.; Milekovic, T.; Asboth, L.; Torres, R. F.; Vachicouras, N.; Liu, Q.; Pavlova, N.; Duis, S.; Larmagnac, A.; Voros, J.; Micera, S.; Suo, Z.; Courtine, G.; Lacour, S. P. *Science* **2015**, *347*, 159.
6. Lim, S.; Son, D.; Kim, J.; Lee, Y. B.; Song, J.; Choi, S.; Lee, D. J.; Kim, J. H.; Lee, M.; Hyeon, T.; Kim, D. –H. *Adv. Funct. Mater*. **2015**, *25*, 375.
7. Kim, D. –H.; Lu, N.; Ma, R.; Kim, Y. –S.; Kim, R. –H.; Wang, S.; Wu, J.; Won, S. M.; Tao, H.; Islam, A.; Yu, K. J.; Kim, T. –i.; Chowdhury, R.; Ying,

M.; Xu, L.; Li, M.; Chung, H. –J.; Keum, H.; McCormick, M.; Liu, P.; Zhang, Y. –W.; Omenetto, F. G.; Huang, Y.; Coleman, T.; Rogers, J. A. *Science* **2011**, *333*, 838.

8. Merletti, R.; Farina, D. *Phil. Trans. R. Soc. A*. **2009**, *367*, 357.
9. Weir, F. F.; Troyk, P. R.; DeMichele, G. A.; Kerns, D. A.; Schorsch, J. F.; Maas, H. *IEEE Trans. Biomed. Eng*. **2008**, *56*, 159
10. Normann, R.; McDonnall, D.; Clark, G. *Conf. Proc. IEEE. Eng. Med. Biol. Soc*. **2005**, *7*, 7644
11. Xu, L.; Gutbrod, S. R.; Bonifas, A. P.; Su, Y.; Sulkin, M. S.; Lu, N.; Chung, H. J.; Jang, K. I.; Liu, Z.; Ying, M.; Lu, C.; Webb, R. C.; Kim, J. –S.; Laughner, J. I.; Cheng, H.; Liu, Y.; Ameen, A.; Jeong, J. –W.; Kim, G. –T.; Huang, Y.; Efimov, I. R.; Rogers, J. A. *Nat. Commun*. **2014**, *5*, 3329
12. Kim, D. –H.; Lu, N.; Ma, R.; Kim, Y. –S.; Kim, R. –H.; Wang, S.; Wu, J.; Won, S. M.; Tao, H.; Islam, A.; Yu, K. J.; Kim, T. –i.; Chowdhury, R.; Ying, M.; Xu, L.; Li, M.; Chung, H. –J.; Keum, H.; McCormick, M.; Liu, P.; Zhang, Y. –W.; Omenetto, F. G.; Huang, Y.; Coleman, T.; Rogers, J. A. *Science* **2011**, *333*, 838
13. Kim, J.; Lee, M.; Shim, H. J.; Ghaffari, R.; Cho, H. R.; Son, D.; Jung, Y. H.; Soh, M.; Choi, C.; Jung, S.; Chu, K.; Jeon, D.; Lee, S. –T.; Kim, J. H.; Choi, S. H.; Hyeon, T.; Kim, D. –H. *Nat. Commun*. **2014**, *5*, 5747.
14. Sekitani, T.; Zschieschang, U.; Klauk, H.; Someya, T. *Nat. Mater*. **2010**, *9*, 1015

15. Kuribara, K.; Wang, H.; Uchiyama, N.; Fukuda, K.; Yokota, T.; Zschieschang, U.; Jaye, C.; Fischer, D.; Klauk, H.; Yamamoto, T.; Takimiya, K.; Ikeda, M.; Kuwabara, H.; Sekitani, T.; Loo, Y. –L.; Someya, T. *Nat. Commn*. **2012**, *3*, 723.
16. Khodagholy, D.; Gelinas, J. N.; Thesen, T.; Doyle, W.; Devinsky, O.; Malliaras, G. G.; Buzasaki, G. *Nat. Neurosci*. **2015**, *18*, 310.
17. Viventi, J.; Kim, D. –H.; Vigeland, L.; Frecheter, E. S.; Blanco, J. A.; Kim, Y. –S.; Avrin, A. E.; Tiruvadi, V. R.; Hwang, S. –W.; Vanleer, A. C.; Wulsin, D. F.; Davis, K.; Gelber, C. E.; Palmer, L.; Spiegel, J. V.; Wu, J.; Xiao, J.; Huang, Y.; Contreras, D.; Rogers, J. A.; Litt, B. *Nat. Neurosci*. **2011**, *14*, 1599.
18. Kim, D. –H.; Viventi, J.; Amsden, J. J.; Xiao, J.; Vigeland, L.; Kim, Y. –S.; Blanco, J. A.; Panilaitis, B.; Frechette, E. S.; Contreras, D.; Kaplan, D. L.; Omenetto, F. G.; Huang, Y.; Hwang, K. C.; Zakin, M. R.; Litt, B.; Rogers, J. A. *Nat. Mater.* **2010**, *9*, 511.
19. LaVan, D. A.; McGuire, T.; Langer, R. *Nat. Biotechnol*. **2003**, *21*, 1184.
20. Son, D.; Lee, J.; Lee, D. J.; Ghaffari, R.; Yun, S.; Kim, S. J.; Lee, J. E.; Cho, H. R.; Yoon, S.; Yang, S.; Lee, S.; Qiao, S.; Ling, D.; Shin, S.; Song, J. –K.; Kim, J.; Kim, T.; Lee, H.; Kim, J.; Soh, M.; Lee, N.; Hwang, C. S.; Nam, S.; Lu, N.; Hyeon, T.; Choi, S. H.; Kim, D. –H. *ACS Nano* **2015**, *9*, 5937.
21. Couvreur, P. *Nat. Nanotechnol*. **2014**, *9*, 874.
22. Brudno, Y.; Silva, E. A.; Kearney, C. J.; Lewin, S. A.; Miller, A.; Martinick,

K. D.; Aizenber, M.; Mooney, D. J. *Proc. Natl. Acad. Sci. U. S. A.* **2014**, *111*, 12722.

23. Pabbruwe, M. B.; Esfandiari, E.; Kafienah, W.; Tarlton, J. F.; Hollander, A. P. *Biomaterials* **2009**, *30*, 4277.
24. Cosgrove, B. D.; Gilbert, P. M.; Porpiglia, E.; Mourkioti, F.; Lee, S. P.; Corbel, S. Y.; Llewellyn, M. E.; Delp, S. L.; Blau, H. M. *Nat. Med*. **2014**, *20*, 255.
25. Chong, J. J.; Yang, X.; Don, C. W.; Minami, E.; Liu, Y. W.; Weyers, J. J.; Mahoney, W. M.; Van Biber, B.; Cook, S. M.; Palpant, N. J.; Gantz, J. A.; Fugate, J. A.; Muskheli, V.; Gough, G. M.; Vogel, K. W.; Astley, C. A.; Hotchkiss, C. E.; Baldessari, A.; Pabon, L.; Reinecke, H.; Gill, E. A.; Nelson, V.; Kiem, H. –P.; Laflamme, M. A.; Murry, C. E. *Nature* **2014**, *510*, 273.
26. Li, J. Y.; Christophersen, N. S.; Hall, V.; Soulet, D.; Brundin, P. *Trends. Neurosci*. **2008**, *31*, 146.
27. Segers, V. F. M.; Lee, R. T. *Nature* **2008**, *451*, 937.
28. Kim, S. J.; Cho, H. R.; Cho, K. W.; Qiao, S.; Rhim, J. S.; Soh, M.; Kim, T.; Choi, M. K.; Choi, C.; Park, I.; Hwang, N. S.; Hyeon, T.; Choi, S. H.; Lu, N.; Kim, D. –H. *ACS Nano* **2015**, *9*, 2677.
29. Stafford, C. M.; Harrison, C.; Beers, K. L.; Karim, A.; Amis, E. J.; VanLandingham, M. R.; Kim, H. C.; Volksen, W.; Miller, R. D.; Simonyi, E. E. *Nat. Mater*. **2004**, *3*, 545.

30. Lacour, S. P.; Jones, J.; Wagner, S.; Li, T.; Suo, Z. *Proc. IEEE* **2005**, *93*, 1459.
31. Garrett, W. E.; Safran, M. R.; Seaber, A. V.; Gilsson, R. R.; Ribbeck, B. M. *Am. J. Sports. Med*. **1987**, *5*, 448.
32. Rassier, D. E.; Maclntosh, B. R.; Herzog, W. *J. Appl. Phys*. **1999**, *86*, 1445.

국문 초록

근육질환진단을 위한

이식형 세포-그래핀 디바이스

근육 질환 진단에서 근육의 생체신호 즉, 근전도를 측정하는것은 매우 중요하다. 특히 근육경직, 근육감소증과 같은 근육질환을 긴 시간 동안 근전도 측정이 질환 진단에서 기초적인 방법이다. 근전도 센서 같은 경우 피부위에서 측정하는 것도 있지만 바늘이나 마크로칩으로 만들어 근육 내에서 측정하는 것이 더욱 정확하다. 하지만 근육 내에서 측정으로 위한 장치들은 딱딱하기 때문에 장치 이식을 하거나 오랜기간 동안의 측정이 어려웠다. 또한 부드럽고 굴곡이 심한 근육조

직이 이식된 딱딱한 장치 때문에 손상이 일어나고 환자들에게 불편을 주었다. 따라서 부드럽고 쉽게 늘어날수 있는 이식형 디바이스를 만들어 생체내에서도 불편함 없이 장기간 동안 근육조직의 생체신호를 측정고자 하는 요구가 증가하고 있다. 본 연구에서는 생체내 주름모양을 본 딴 구조와 구불구불한-메쉬 패턴의 그래핀 전극은 디바이스가 최대 40%까지 늘어나게 하며, 그 위 근육세포를 배양해 세포시트를 형성하여 세포치료 효과 기능과 근전도 측정 및 전기자극 치료 기능과 더불어 전체적인 디바이스의 기반을 부드러운 소재의 40:1 PDMS를 이용해 근육조직과 conformal contact을 형성 한다. 따라서 장기간 이식으로 인한 근육손상을 방지하고 환자의 불편함을 덜어줄 수 있는 세포-그래핀 디바이스를 구현하였다.

주요어: 주름모양구조 세포-그래핀, 늘어나는 디바이스, 이식형 디바이스, 생체신호 측정, 근전도 측정

학번: 2014-21598